Angular dependence of the upper critical field in the high-pressure $1T'$ phase of $MoTe_2$

Y. J. Hu,[1] Yuk Tai Chan,[1] Kwing To Lai,[1,*] Kin On Ho,[1] Xiaoyu Guo,[1] Hai-Peng Sun,[2,3,4] K. Y. Yip,[1] Dickon H. L. Ng,[1] Hai-Zhou Lu,[2,3] and Swee K. Goh[1,†]

[1]*Department of Physics, The Chinese University of Hong Kong, Shatin, Hong Kong*
[2]*Shenzhen Institute for Quantum Science and Engineering and Department of Physics, Southern University of Science and Technology, Shenzhen 518055, China*
[3]*Shenzhen Key Laboratory of Quantum Science and Engineering, Shenzhen 518055, China*
[4]*Department of Physics, Harbin Institute of Technology, Harbin 150001, China*

(Received 27 December 2018; published 25 March 2019)

Superconductivity in the type-II Weyl semimetal candidate $MoTe_2$ has attracted much attention due to the possible realization of topological superconductivity. Under applied pressure, the superconducting transition temperature is significantly enhanced, while the structural transition from the high-temperature $1T'$ phase to the low-temperature T_d phase is suppressed. Hence, applying pressure allows us to investigate the dimensionality of superconductivity in $1T'$-$MoTe_2$. We have performed a detailed study of the magnetotransport properties and upper critical field H_{c2} of $MoTe_2$ under pressure. The magnetoresistance (MR) and Hall coefficient of $MoTe_2$ are found to decrease with increasing pressure. In addition, the Kohler's scalings for the MR data above ∼11 kbar show a change of exponent whereas the data at lower pressure can be well scaled with a single exponent. These results are suggestive of a Fermi-surface reconstruction when the structure changes from the T_d to $1T'$ phase. The H_{c2}-temperature phase diagram constructed at 15 kbar, with $H \parallel ab$ and $H \perp ab$, can be satisfactorily described by the Werthamer–Helfand–Hohenberg model with the Maki parameters $\alpha \sim 0.77$ and 0.45, respectively. The relatively large α may stem from a small Fermi surface and a large effective mass of semimetallic $MoTe_2$. The angular dependence of H_{c2} at 15 kbar can be well fit by the Tinkham model, suggesting the two-dimensional nature of superconductivity in the high-pressure $1T'$ phase.

DOI: 10.1103/PhysRevMaterials.3.034201

I. INTRODUCTION

Transition-metal dichalcogenides WTe_2 and $MoTe_2$ have recently been intensively studied owing to their intriguing physical properties [1]. For example, extremely large magnetoresistance (MR) has been reported in both WTe_2 [2] and $MoTe_2$ [3]. Further interests are generated when they are considered as candidates of type-II Weyl semimetals [4–7], which would have a pair of topologically nontrivial Weyl points at the boundary of electron and hole Fermi surfaces. A recent focus on these materials concerns their superconductivity because this opens up the possibility of finding topological superconductivity, which could stabilize exotic Majorana fermions [8]. These features are promising for the development of spintronics devices.

Both WTe_2 and $MoTe_2$ consist of weakly bonded (W/Mo)-Te layers stacked along the c axis. While WTe_2 crystallizes in a noncentrosymmetric orthorhombic T_d phase (space group $Pmn2_1$) at ambient pressure, $MoTe_2$ undergoes a first-order structural transition from a centrosymmetric monoclinic $1T'$ phase (space group $P2_1/m$) to the T_d phase at $T_s \sim 250$ K. At low temperature, a superconducting phase transition can additionally be observed at $T_c \sim 0.1$ K [9]. In contrast, superconductivity in bulk WTe_2 can only be stabilized at high pressure ($\gtrsim$25 kbar) [10–12].

An interesting interplay between structural and superconducting transitions in $MoTe_2$ is revealed upon the application of hydrostatic pressure: T_s can be suppressed to zero at ∼10 kbar, i.e., at high pressure, the T_d phase can be completely removed and the $1T'$ phase takes over. Meanwhile, T_c is rapidly enhanced, leading to a 30-fold increase in T_c (∼4 K) at ∼15 kbar [9,13–16]. A similar enhancement of T_c can also be observed in S-, Se- and Re-doped $MoTe_2$ as well as Te-deficient $MoTe_2$, but T_s is only slightly suppressed before suddenly vanishing with increasing doping or deficiency levels [13,17–19]. Therefore, pressurized $MoTe_2$ presents an opportunity to study the nature of the superconductivity in the $1T'$ phase.

Previous high-pressure studies reported the intrinsic superconductivity in many topological materials, including Cd_3As_2 [20], TaAs [21], TaP [22], $ZrTe_5$ [23], $HfTe_5$ [24], $TaIrTe_4$ [25,26], and YPtBi [27–29]. In particular, the topological semimetal YPtBi has been found to be an unconventional spin-3/2 superconductor, which is beyond the value of spin in triplet superconductors [30]. In $MoTe_2$, the enhanced T_c at high pressure has not been envisaged in previous density-functional theory predictions [31]. This discrepancy may be due to the two-dimensional (2D) nature of the superconductivity in $MoTe_2$. Recently, Heikes *et al.* [14] suggested that applying pressure to $MoTe_2$ would induce the decoupling of Mo-Te layers, leading to a more-2D structure. If this high-pressure superconducting phase is quasi-2D, it would be a possible route to search for topological superconductivity [8]. Thus, it is desirable to gauge both the anisotropy of the normal

*ktlai@phy.cuhk.edu.hk
†skgoh@cuhk.edu.hk

state and the superconducting state under pressure. The case of WTe_2 is particularly instructive: while its crystal structure is of layered nature and hence highly two-dimensional, the electronic structure and the superconducting state (at ∼100 kbar) are practically isotropic. These conclusions for WTe_2 are drawn from quantum oscillations [32–34], angle-resolved photoemission spectroscopy (ARPES) [34,35], and angular dependence of the magnetoresistance [36] for the electronic structure, and the angular dependence of the upper critical field (H_{c2}) for the superconducting state [12]. In this article, we report the anisotropy of the superconductivity in the $1T'$ phase via a measurement of H_{c2} against the field angle down to 30 mK at 15 kbar.

II. EXPERIMENT

Single crystals of $MoTe_2$ were synthesized by using the NaCl-flux method, as described elsewhere [3]. Temperature-dependent electrical transport measurements were performed by a standard four-probe technique in a Bluefors dilution fridge. Hydrostatic pressure dependence was studied by using a piston-cylinder clamp cell with glycerin as the pressure-transmitting medium. The pressure value inside the clamp cell was measured by the zero-field superconducting transition of a piece of Pb placed near the sample. Magnetic-field-dependent transport properties were measured with the aid of a superconducting magnet. Transverse resistivity (Hall resistivity) was obtained by symmetrizing (antisymmetrizing) the field-dependent transport data recorded in both positive and negative field directions. For the measurements of the angular dependence of H_{c2} at 15 kbar, a miniature moissanite anvil cell was used in conjunction with a vector magnet with a maximum horizontal field of 3 T and a maximum vertical field of 5 T. The pressure achieved in the anvil cell was determined by ruby fluorescence spectroscopy at room temperature, and glycerin was also used as the pressure-transmitting medium. The single crystals used (S1-S4) are from the same growth batch.

III. RESULTS AND DISCUSSION

Figure 1(a) shows the temperature dependence of the zero-field electrical resistivity $\rho(T)$ (solid lines) of $MoTe_2$ (S1) at ambient pressure. A pronounced anomaly in $\rho(T)$ is recorded at $T_s \approx 260$ K. This anomaly exhibits a strong hysteresis, signaling a first-order structural transition from the $1T'$ to the T_d phase, which is consistent with previous reports [3,9,13–15]. The residual resistivity ratio (RRR) for this sample (S1) is 170, which is a typical value for all samples used in this study. Figure 1(a) additionally illustrates $\rho(T)$ data at 14 T from 120 to 2 K. Below $T^* = 38$ K, $\rho(T)$ experiences a large enhancement. Consequently, MR at low temperatures is large and reaches 7956% at 14 T and 2 K, indicating the existence of highly mobile carriers.

Figures 1(b) and 1(c) display the zero-field $\rho(T)$ curves under pressure. By increasing pressure, the anomaly associated with T_s, as indicated by the arrow, weakens drastically and becomes difficult to discern from 11 kbar. The low-temperature part of $\rho(T)$ shows the evolution of the superconducting transition under pressure [Fig. 1(c)]. The values of T_c are defined

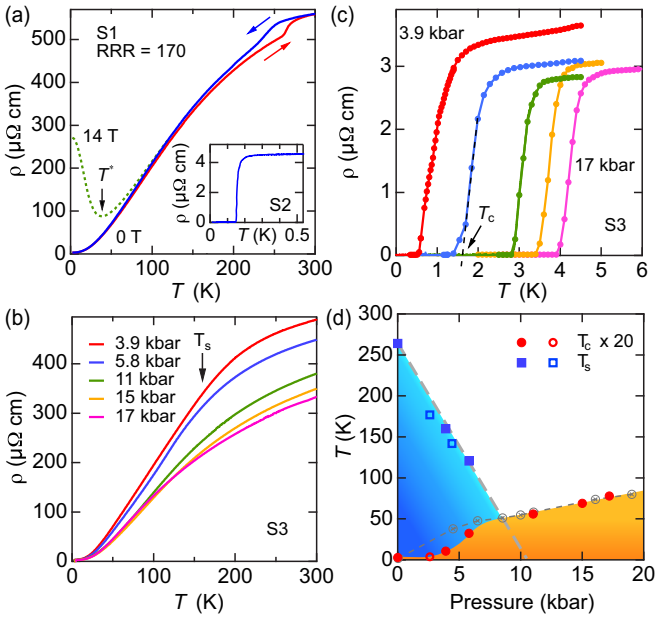

FIG. 1. (a) Temperature dependence of electrical resistivity $\rho(T)$ of $MoTe_2$ (S1) at ambient pressure and zero field (solid curves). The arrows indicate the direction of the temperature sweeps. The dashed curve is $\rho(T)$ at 14 T, showing a field-induced upturn at T^*. The inset shows the superconducting transition of S2 at ambient pressure. (b) Pressure dependence of $\rho(T)$ of S3. (c) The superconducting transition of S3 at different pressures. The definition of T_c is indicated. (d) Temperature-pressure phase diagram of $MoTe_2$. The solid symbols represent the data from S3. The open symbols are data from other pressure cell runs. The gray points are data from Ref. [16].

as the horizontal intercepts of the straight line extrapolated from the transition region [see dashed line in Fig. 1(c)]. Figure 1(d) summarizes the pressure dependence of T_s and T_c: upon increasing pressure, T_s decreases and extrapolates linearly to 0 K at 11 kbar while T_c is significantly enhanced. The resultant temperature-pressure phase diagram is generally consistent with previous studies [9,13–16]. In particular, zero resistance has been observed in the superconducting state at all pressures investigated [Fig. 1(c)], in contrast with several reports which covered the same pressure range [14,15].

In the established temperature-pressure phase diagram, we are able to track the pressure evolution of the electronic structure via magnetotransport. Figures 2(a) and 2(b) show the field dependence of the transverse resistivity ρ_{xx} and the Hall resistivity ρ_{xy} at 30 mK at different pressures, respectively. The superconducting transition can be seen in both ρ_{xx} and ρ_{xy} at all pressures. At low temperatures, because of the superconducting transition, $\rho_{xx} = 0$. Therefore, $\rho_{xx}(0\,\mathrm{T})$ is extrapolated from the polynomial fitting of the normal-state data. ρ_{xy} is determined by first antisymmetrizing the measured voltage at positive and negative field, and converted by considering the geometry of the sample. The tiny peak at low field, which is close to the superconducting transition, might be an experimental artifact and is excluded from the analysis. Figure 2(c) shows the pressure dependence of MR [$= \Delta\rho_{xx}/\rho(0)$] at 13 T and 30 mK derived from Fig. 2(a). Figure 2(d) displays the pressure dependence of the Hall coefficient R_H at 30 mK, which is extracted by fitting the ρ_{xy} data in Fig. 2(b) with

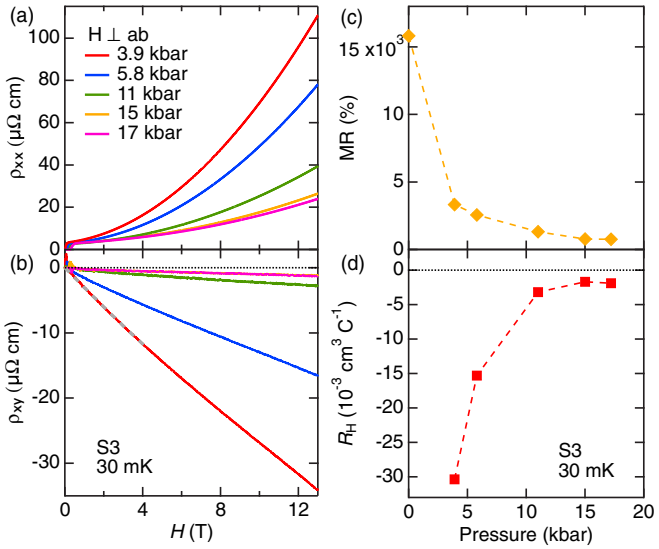

FIG. 2. Field dependence of (a) transverse resistivity ρ_{xx} and (b) Hall resistivity ρ_{xy} for S3 at 30 mK at different pressures. The magnetic-field direction is perpendicular to the *ab* plane. The gray dashed line in panel (b) is the fitting of $\rho_{xy} = R_H H + \beta H^3$ to normal-state data below 4 T. (c) Pressure dependence of the magnetoresistance (MR) at 13 T and 30 mK. (d) Pressure dependence of Hall coefficient R_H at 30 mK.

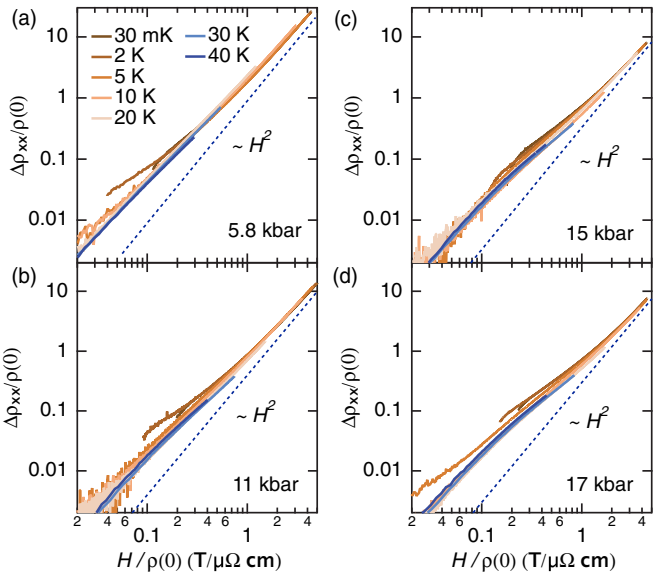

FIG. 3. Kohler's plots of S3 at (a) 5.8 kbar, (b) 11 kbar, (c) 15 kbar, and (d) 17 kbar. The dashed lines indicate the H^2 dependence.

$\rho_{xy} = R_H H + \beta H^3$, where βH^3 accounts for the small nonlinearity in ρ_{xy}. Only the normal-state data below 4 T are used for this analysis [see gray dashed line in Fig. 2(b)]. When pressure is applied, MR(13 T, 30 mK) first decreases rapidly before levelling off above ∼11 kbar, indicating a drastic decrease of carrier mobilities. Meanwhile, a significant initial suppression of $|R_H(30\ \text{mK})|$ is observed, followed by a nearly constant $|R_H(30\ \text{mK})|$ above the same pressure (∼11 kbar). $R_H(30\ \text{mK})$ is negative for all pressures studied, indicating that electrons dominate the electrical transport, while the relative size of electron Fermi pockets increases with pressure. The relatively weak pressure dependence of $|R_H(30\ \text{mK})|$ and MR(13 T, 30 mK) above ∼11 kbar is consistent with the removal of the T_d phase.

Figure 3 shows the Kohler plots at 5.8, 11, 15, and 17 kbar, respectively. MR against $H/\rho(0)$ is plotted, where $\rho(0)$ is the zero-field resistivity at a fixed temperature [37]. At 5.8 kbar, the data at different temperatures collapse onto a single curve which is nearly quadratic in field, indicating that Kohler's rule is obeyed. The observation of the Kohler's rule has also been demonstrated at ambient pressure [38]. However, at 15 and 17 kbar, Kohler's scalings are less satisfied and, when plotted on log-log scales, a slope change is detected. The slope change is also noticeable at 11 kbar [Fig. 3(b)], although the feature is much weaker. This indicates a change in the field exponent and is reminiscent of the case of LaSb [39], in which a similar change of exponent is noticeable in the Kohler plot at ambient pressure. In LaSb, this behavior is attributed to the different mobilities associated with different electron Fermi pockets. Thus, if the change of the field exponent detected in $MoTe_2$ at $\geqslant$11 kbar is similarly rooted on the details of Fermiology, the Fermi surfaces could be different from those at <11 kbar. This is consistent with the pressure evolution of $|R_H(30\ \text{mK})|$ and the analysis of Ref. [15], in which they discovered that a four-band model is needed to describe their magnetotransport data above ∼10 kbar, in contrast with the more conventional two-band model applicable for their data at low pressures. The difference of MR between the low and high pressure is again suggestive of the electronic structure reconstruction from the T_d phase to the $1T'$ phase.

Next, we discuss the superconducting state in the high-pressure $1T'$ phase. In the $1T'$ phase, T_c is significantly enhanced, making it easier to investigate the anisotropy of the superconducting state through the measurements of H_{c2} [12,29,40–45]. We have performed the H_{c2} study on $MoTe_2$ (S4) at 15 kbar, which is in the $1T'$ phase according to our phase diagram [see Fig. 1(d)]. Figure 4 illustrates the field-temperature phase diagram $H_{c2}(T)$ of $MoTe_2$ at 15 kbar, with $H \parallel ab$ and $H \perp ab$. The raw resistivity data from which these $H_{c2}(T)$ data are determined can be found in the Supplemental Material [37]. According to the Werthamer–Helfand–Hohenberg (WHH) theory [46] for a type-II superconductor in the dirty limit, the orbital-limited upper critical field is given by

$$H_{c2}^{\text{orb}}(0) = -0.693 T_c \left.\frac{dH_{c2}}{dT}\right|_{T=T_c}. \quad (1)$$

The initial slope $(dH_{c2}/dT)_{T=T_c}$ is −0.26 T/K and −0.12 T/K for $H \parallel ab$ and $H \perp ab$, respectively. Thus, $H_{c2}^{\text{orb}}(0)$ are estimated as 0.65 and 0.29 T, respectively, which are larger than the experimental data at the 0 K limit $[H_{c2}(0)]$. The suppression of $H_{c2}(0)$ is more pronounced with $H \parallel ab$. To account for this suppression, we include the Maki parameter α. The WHH formula with a finite α is used to fit $H_{c2}(T)$, as displayed in Fig. 4 (solid lines). With $\alpha = 0.77$ for the $H \parallel ab$ direction and $\alpha = 0.45$ for the $H \perp ab$ direction, we are able to describe the $H_{c2}(T)$ data very well.

The Maki parameter α can be written as

$$\alpha = \sqrt{2} H_{c2}^{\text{orb}}(0)/H_P(0) \sim m^* \Delta(0)/E_F, \quad (2)$$

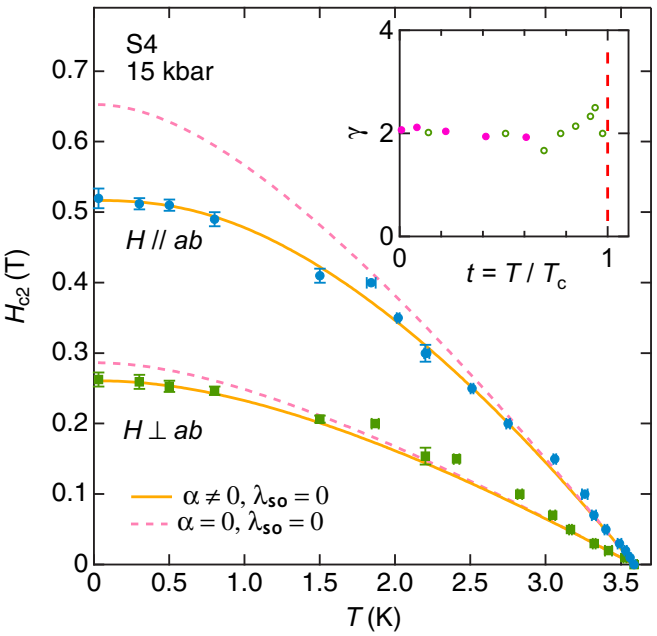

FIG. 4. Field-temperature phase diagram of S4 at 15 kbar, with $H \parallel ab$ and $H \perp ab$. The data (symbols) are measured by both temperature sweeps and field sweeps. The solid and dashed lines are the fits using the WHH model with the Maki parameter $\alpha \neq 0$ and $\alpha = 0$, respectively. The inset displays the temperature dependence of the anisotropy factor $\gamma = H_{c2}(0^\circ)/H_{c2}(90^\circ)$. The solid and open symbols represent the data from the rotation studies and H_{c2} data in the main panel, respectively.

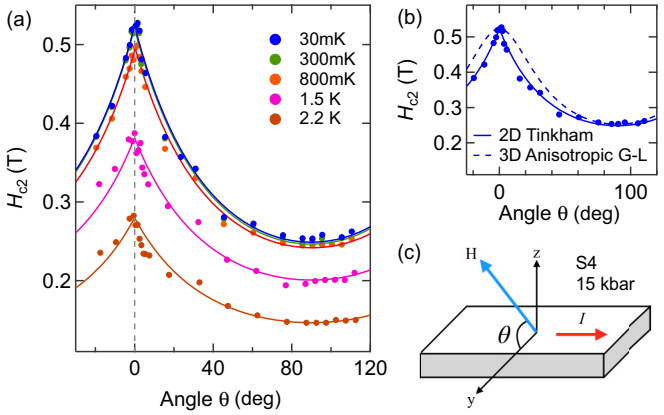

FIG. 5. (a) $H_{c2}(\theta)$ of S4 at 15 kbar at different temperatures. The solid lines are fits using the Tinkham model. (b) Comparison between the 2D Tinkham model (solid line) and the three-dimensional anisotropic mass model (dashed line) for $H_{c2}(\theta)$ at 30 mK. (c) Arrangement of sample and magnetic field. The z axis is parallel to the c axis of the sample, while the y axis lies in the ab plane. The current is always perpendicular to the magnetic field.

where $H_P(0)$ and $\Delta(0)$ are the Pauli-limiting upper critical field and the magnitude of the superconducting gap at the zero-temperature limit, respectively, and E_F is the Fermi energy. Thus, α describes the relative strength of the orbital and spin-paramagnetic (Zeeman) effects. For a conventional metal, E_F is $\sim$1 eV while $\Delta(0)$ is $\sim$1 meV, α is usually much smaller than 1. Therefore, the value of $\alpha = 0.77$ is unexpected, indicating a non-negligible spin-paramagnetic contribution to the pair breaking. As stipulated in Eq. (2), an enhanced spin-paramagnetic contribution can come from a small Fermi surface, a large effective mass, or a large $\Delta(0)$. Since T_c is low in this system, $\Delta(0)$ alone cannot drive the enhancement of α. However, the importance of electron-electron correlations has recently been highlighted [47,48]. Together with the semimetallic nature of $MoTe_2$, the enhancement of α can probably be traced back to the low E_F and high m^*. Another possible scenario is that the suppression of H_{c2} could be attributed by the multiband effect with large tunneling between the valleys in Dirac and Weyl semimetals, according to the recent calculation [49].

We now assess the anisotropy of the superconductivity in the $1T'$ phase via a full angular dependence of the upper critical field $H_{c2}(\theta)$ at selected temperatures between 30 mK ($0.008T_c$) and 2.2 K ($0.61T_c$), as illustrated in Fig. 5(a). The definition of the angle θ is shown in Fig. 5(c), where $\theta = 0^\circ$ (90°) corresponds to $H \parallel ab$ ($H \perp ab$). At all temperatures studied, $H_{c2}(\theta)$ exhibits a distinct cusp around $H \parallel ab$, which can be well described by the Tinkham model for 2D superconductivity [50]:

$$\left|\frac{H_{c2}(\theta)\sin(\theta)}{H_{c2}(90^\circ)}\right| + \left[\frac{H_{c2}(\theta)\cos(\theta)}{H_{c2}(0^\circ)}\right]^2 = 1. \quad (3)$$

Figure 5(b) compares the 2D Tinkham model and the three-dimensional (3D) anisotropic mass Ginzburg–Landau (G-L) model. The 3D anisotropic mass G-L model clearly fails to capture the cusp at 0°. Therefore, the superconductivity in $1T'$ $MoTe_2$ is identified to be two-dimensional. This is in sharp contrast with the case of WTe_2 at 98.5 kbar, in which $H_{c2}(\theta)$ can be described by the 3D anisotropic mass G-L model [12].

Despite the success of the Tinkham model in describing $H_{c2}(\theta)$, the anisotropy factor $\gamma = H_{c2}(0^\circ)/H_{c2}(90^\circ)$ is 2.1, which is rather low (inset of Fig. 4) and only slightly larger than the γ of 1.7 established in WTe_2 [12]. Furthermore, the in-plane and out-of-plane coherence lengths at the zero-temperature limit, $\xi_\parallel$ and $\xi_\perp$, respectively, can be extracted from the H_{c2} data, giving $\xi_\parallel = 35.6$ nm and $\xi_\perp = 17.8$ nm. The value of $\xi_\perp$ is much larger than the interlayer distance, which is surprising considering the 2D nature of the superconductivity. In fact, the present case is reminiscent of CaAlSi, a superconductor with a MgB_2-like structure. In CaAlSi, $H_{c2}(\theta)$ also follows the Tinkham model with a rather low anisotropy factor [51]. There, $\xi_\perp$ is also larger than the thickness of the normal layer, and γ ranges from $\sim$2 (similar to the present study) at $0.5T_c$ to $\sim$3.5 at $\sim 0.9T_c$. The large out-of-plane coherence length for a 2D superconductor remains a puzzle and has to be reconciled in the future.

IV. CONCLUSIONS

In summary, we have constructed the temperature-pressure phase diagram of $MoTe_2$ and investigated the anisotropy of superconductivity of the high-pressure $1T'$ phase at 15 kbar. The first-order structural phase transition temperature T_s (from the high-temperature $1T'$ phase to the low-temperature T_d phase)

is suppressed with applied pressure and vanishes at ∼11 kbar, while the superconducting transition temperature T_c is significantly enhanced. With the application of pressure, the magnetoresistance (MR) and Hall coefficient decrease and saturate to low values at >11 kbar. The Kohler scaling can well describe the MR data at all pressures. Meanwhile, a change of exponent is observed at high pressure, suggestive of a Fermi-surface reconstruction. Thus, the temperature-pressure phase diagram, together with the magnetotransport measurements, support the conclusion that the superconductivity at >11 kbar is in the $1T'$ phase. Using the Werthamer–Helfand–Hohenberg model with the inclusion of the Maki parameter α, the temperature dependence of the upper critical field H_{c2} at 15 kbar, obtained at $H \parallel ab$ and $H \perp ab$, can be nicely described with $\alpha = 0.77$ for $H \parallel ab$ and $\alpha = 0.45$ for $H \perp ab$. These surprisingly large α indicate the presence of the spin-paramagnetic effect. This behavior may be related to the low Fermi energy in the semimetallic $1T'$-$MoTe_2$, and the large effective mass due to the non-negligible electron-electron correlation. Finally, the angular dependence of H_{c2} can be described by the Tinkham model over a wide temperature range, indicating that the dimensionality of the superconducting state in the high-pressure $1T'$ phase is two-dimensional in nature.

ACKNOWLEDGMENTS

We acknowledge technical support from Qun Niu, and financial support from Research Grants Council of Hong Kong (GRF/14300418, GRF/14301316, GRF/14300117), CUHK Direct Grant (4053223, 4053299), National Natural Science Foundation of China (11504310, 11574127), Guangdong Innovative and Entrepreneurial Research Team Program (2016ZT06D348), National Key R&D Program (2016YFA0301700) and Science, Technology, and Innovation Commission of Shenzhen Municipality (ZDSYS20170303165926217 and JCYJ20170412152620376).

Y.J.H. and Y.T.C. contributed equally to this work.

[1] B. Yan and C. Felser, Annu. Rev. Condens. Matter Phys. **8**, 337 (2017).

[2] M. N. Ali, J. Xiong, S. Flynn, J. Tao, Q. D. Gibson, L. M. Schoop, T. Liang, N. Haldolaarachchige, M. Hirschberger, N. P. Ong, and R. J. Cava, Nature (London) **514**, 205 (2014).

[3] D. H. Keum, S. Cho, J. H. Kim, D.-H. Choe, H.-J. Sung, M. Kan, H. Kang, J.-Y. Hwang, S. Kim, H. Yang, K. J. Chang, and Y. H. Lee, Nat. Phys. **11**, 482 (2015).

[4] A. A. Soluyanov, D. Gresch, Z. Wang, Q. Wu, M. Troyer, X. Dai, and B. A. Bernevig, Nature (London) **527**, 495 (2015).

[5] Y. Wu, D. Mou, N. H. Jo, K. Sun, L. Huang, S. L. Bud'ko, P. C. Canfield, and A. Kaminski, Phys. Rev. B **94**, 121113 (2016).

[6] K. Deng, G. Wan, P. Deng, K. Zhang, S. Ding, E. Wang, M. Yan, H. Huang, H. Zhang, Z. Xu, J. Denlinger, A. Fedorov, H. Yang, W. Duan, H. Yao, Y. Wu, S. Fan, H. Zhang, X. Chen, and S. Zhou, Nat. Phys. **12**, 1105 (2016).

[7] J. Jiang, Z. K. Liu, Y. Sun, H. F. Yang, C. R. Rajamathi, Y. P. Qi, L. X. Yang, C. Chen, H. Peng, C.-C. Hwang, S. Z. Sun, S.-K. Mo, I. Vobornik, J. Fujii, S. S. P. Parkin, C. Felser, B. H. Yan, and Y. L. Chen, Nat. Commun. **8**, 13973 (2017).

[8] M. Sato and Y. Ando, Rep. Prog. Phys. **80**, 076501 (2017).

[9] Y. Qi, P. G. Naumov, M. N. Ali, C. R. Rajamathi, W. Schnelle, O. Barkalov, M. Hanfland, S.-C. Wu, C. Shekhar, Y. Sun, V. Süß, M. Schmidt, U. Schwarz, E. Pippel, P. Werner, R. Hillebrand, T. Förster, E. Kampert, S. Parkin, R. J. Cava, C. Felser, B. Yan, and S. A. Medvedev, Nat. Commun. **7**, 11038 (2016).

[10] X.-C. Pan, X. Chen, H. Liu, Y. Feng, Z. Wei, Y. Zhou, Z. Chi, L. Pi, F. Yen, F. Song, X. Wan, Z. Yang, B. Wang, G. Wang, and Y. Zhang, Nat. Commun. **6**, 7805 (2015).

[11] D. Kang, Y. Zhou, W. Yi, C. Yang, J. Guo, Y. Shi, S. Zhang, Z. Wang, C. Zhang, S. Jiang, A. Li, K. Yang, Q. Wu, G. Zhang, L. Sun, and Z. Zhao, Nat. Commun. **6**, 7804 (2015).

[12] Y. T. Chan, P. L. Alireza, K. Y. Yip, Q. Niu, K. T. Lai, and S. K. Goh, Phys. Rev. B **96**, 180504 (2017).

[13] H. Takahashi, T. Akiba, K. Imura, T. Shiino, K. Deguchi, N. K. Sato, H. Sakai, M. S. Bahramy, and S. Ishiwata, Phys. Rev. B **95**, 100501 (2017).

[14] C. Heikes, I.-L. Liu, T. Metz, C. Eckberg, P. Neves, Y. Wu, L. Hung, P. Piccoli, H. Cao, J. Leao, J. Paglione, T. Yildirim, N. P. Butch, and W. Ratcliff, Phys. Rev. Mater. **2**, 074202 (2018).

[15] S. Lee, J. Jang, S.-I. Kim, S.-G. Jung, J. Kim, S. Cho, S. W. Kim, J. Y. Rhee, K.-S. Park, and T. Park, Sci. Rep. **8**, 13937 (2018).

[16] Z. Guguchia, F. von Rohr, Z. Shermadini, A. T. Lee, S. Banerjee, A. R. Wieteska, C. A. Marianetti, B. A. Frandsen, H. Luetkens, Z. Gong, S. C. Cheung, C. Baines, A. Shengelaya, G. Taniashvili, A. N. Pasupathy, E. Morenzoni, S. J. L. Billinge, A. Amato, R. J. Cava, R. Khasanov, and Y. J. Uemura, Nat. Commun. **8**, 1082 (2017).

[17] F. C. Chen, X. Luo, R. C. Xiao, W. J. Lu, B. Zhang, H. X. Yang, J. Q. Li, Q. L. Pei, D. F. Shao, R. R. Zhang, L. S. Ling, C. Y. Xi, W. H. Song, and Y. P. Sun, Appl. Phys. Lett. **108**, 162601 (2016).

[18] S. Cho, S. H. Kang, H. S. Yu, H. W. Kim, W. Ko, S. W. Hwang, W. H. Han, D.-H. Choe, Y. H. Jung, K. J. Chang, Y. H. Lee, H. Yang, and S. W. Kim, 2D Mater. **4**, 021030 (2017).

[19] M. Mandal, S. Marik, K. P. Sajilesh, Arushi, D. Singh, J. Chakraborty, N. Ganguli, and R. P. Singh, Phys. Rev. Mater. **2**, 094201 (2018).

[20] L. He, Y. Jia, S. Zhang, X. Hong, C. Jin, and S. Li, npj Quantum Mater. **1**, 16014 (2016).

[21] Y. Zhou, P. Lu, Y. Du, X. Zhu, G. Zhang, R. Zhang, D. Shao, X. Chen, X. Wang, M. Tian, J. Sun, X. Wan, Z. Yang, W. Yang, Y. Zhang, and D. Xing, Phys. Rev. Lett. **117**, 146402 (2016).

[22] Y. Li, Y. Zhou, Z. Guo, F. Han, X. Chen, P. Lu, X. Wang, C. An, Y. Zhou, J. Xing, G. Du, X. Zhu, H. Yang, J. Sun, Z. Yang, W. Yang, H.-K. Mao, Y. Zhang, and H.-H. Wen, npj Quantum Mater. **2**, 66 (2017).

[23] Y. Zhou, J. Wu, W. Ning, N. Li, Y. Du, X. Chen, R. Zhang, Z. Chi, X. Wang, X. Zhu, P. Lu, C. Ji, X. Wan, Z. Yang, J. Sun, W. Yang, M. Tian, Y. Zhang, and H.-k. Mao, Proc. Natl. Acad. Sci. USA **113**, 2904 (2016).

[24] Y. Qi, W. Shi, P. G. Naumov, N. Kumar, W. Schnelle, O. Barkalov, C. Shekhar, H. Borrmann, C. Felser, B. Yan, and S. A. Medvedev, Phys. Rev. B **94**, 054517 (2016).

[25] S. Cai, E. Emmanouilidou, J. Guo, X. Li, Y. Li, K. Yang, A. Li, Q. Wu, N. Ni, and L. Sun, Phys. Rev. B **99**, 020503 (2019).
[26] Y. Xing *et al.*, arXiv:1805.10883.
[27] M. Meinert, Phys. Rev. Lett. **116**, 137001 (2016).
[28] N. P. Butch, P. Syers, K. Kirshenbaum, A. P. Hope, and J. Paglione, Phys. Rev. B **84**, 220504 (2011).
[29] T. V. Bay, T. Naka, Y. K. Huang, and A. de Visser, Phys. Rev. B **86**, 064515 (2012).
[30] H. Kim, K. Wang, Y. Nakajima, R. Hu, S. Ziemak, P. Syers, L. Wang, H. Hodovanets, J. D. Denlinger, P. M. R. Brydon, D. F. Agterberg, M. A. Tanatar, R. Prozorov, and J. Paglione, Sci. Adv. **4**, eaao4513 (2018).
[31] M. Rifliková, R. Martoňák, and E. Tosatti, Phys. Rev. B **90**, 035108 (2014).
[32] P. L. Cai, J. Hu, L. P. He, J. Pan, X. C. Hong, Z. Zhang, J. Zhang, J. Wei, Z. Q. Mao, and S. Y. Li, Phys. Rev. Lett. **115**, 057202 (2015).
[33] Z. Zhu, X. Lin, J. Liu, B. Fauqué, Q. Tao, C. Yang, Y. Shi, and K. Behnia, Phys. Rev. Lett. **114**, 176601 (2015).
[34] Y. Wu, N. H. Jo, D. Mou, L. Huang, S. L. Bud'ko, P. C. Canfield, and A. Kaminski, Phys. Rev. B **95**, 195138 (2017).
[35] D. Di Sante, P. K. Das, C. Bigi, Z. Ergönenc, N. Gürtler, J. A. Krieger, T. Schmitt, M. N. Ali, G. Rossi, R. Thomale, C. Franchini, S. Picozzi, J. Fujii, V. N. Strocov, G. Sangiovanni, I. Vobornik, R. J. Cava, and G. Panaccione, Phys. Rev. Lett. **119**, 026403 (2017).
[36] L. R. Thoutam, Y. L. Wang, Z. L. Xiao, S. Das, A. Luican-Mayer, R. Divan, G. W. Crabtree, and W. K. Kwok, Phys. Rev. Lett. **115**, 046602 (2015).
[37] See Supplemental Material at http://link.aps.org/supplemental/10.1103/PhysRevMaterials.3.034201 for magnetoresistance data at 5.8 kbar, 11 kbar, 15 kbar, and 17 kbar plotted against the magnetic field, and the raw resistivity data for the determination of the upper critical field.
[38] Q. L. Pei, W. J. Meng, X. Luo, H. Y. Lv, F. C. Chen, W. J. Lu, Y. Y. Han, P. Tong, W. H. Song, Y. B. Hou, Q. Y. Lu, and Y. P. Sun, Phys. Rev. B **96**, 075132 (2017).
[39] F. Han, J. Xu, A. S. Botana, Z. L. Xiao, Y. L. Wang, W. G. Yang, D. Y. Chung, M. G. Kanatzidis, M. R. Norman, G. W. Crabtree, and W. K. Kwok, Phys. Rev. B **96**, 125112 (2017).
[40] Y. C. Chan, K. Y. Yip, Y. W. Cheung, Y. T. Chan, Q. Niu, J. Kajitani, R. Higashinaka, T. D. Matsuda, Y. Yanase, Y. Aoki, K. T. Lai, and S. K. Goh, Phys. Rev. B **97**, 104509 (2018).
[41] S. K. Goh, Y. Mizukami, H. Shishido, D. Watanabe, S. Yasumoto, M. Shimozawa, M. Yamashita, T. Terashima, Y. Yanase, T. Shibauchi, A. I. Buzdin, and Y. Matsuda, Phys. Rev. Lett. **109**, 157006 (2012).
[42] M. Shimozawa, S. K. Goh, R. Endo, R. Kobayashi, T. Watashige, Y. Mizukami, H. Ikeda, H. Shishido, Y. Yanase, T. Terashima, T. Shibauchi, and Y. Matsuda, Phys. Rev. Lett. **112**, 156404 (2014).
[43] M. J. Naughton, R. C. Yu, P. K. Davies, J. E. Fischer, R. V. Chamberlin, Z. Z. Wang, T. W. Jing, N. P. Ong, and P. M. Chaikin, Phys. Rev. B **38**, 9280 (1988).
[44] Q. L. He, H. Liu, M. He, Y. H. Lai, H. He, G. Wang, K. T. Law, R. Lortz, J. Wang, and I. K. Sou, Nat. Commun. **5**, 4247 (2014).
[45] S. Yonezawa, K. Tajiri, S. Nakata, Y. Nagai, Z. Wang, K. Segawa, Y. Ando, and Y. Maeno, Nat. Phys. **13**, 123 (2017).
[46] N. R. Werthamer, E. Helfand, and P. C. Hohenberg, Phys. Rev. **147**, 295 (1966).
[47] N. Xu, Z. W. Wang, A. Magrez, P. Bugnon, H. Berger, C. E. Matt, V. N. Strocov, N. C. Plumb, M. Radovic, E. Pomjakushina, K. Conder, J. H. Dil, J. Mesot, R. Yu, H. Ding, and M. Shi, Phys. Rev. Lett. **121**, 136401 (2018).
[48] N. Aryal and E. Manousakis, Phys. Rev. B **99**, 035123 (2019).
[49] B. Rosenstein, B. Y. Shapiro, D. Li, and I. Shapiro, Europhys. Lett. **124**, 27004 (2018).
[50] M. Tinkham, Phys. Rev. **129**, 2413 (1963).
[51] A. K. Ghosh, M. Tokunaga, and T. Tamegai, Phys. Rev. B **68**, 054507 (2003).